

## NO-Releasing Compounds | Very Important Paper |

## VIP Organometallic Ruthenium Nitrosyl Obtained by C–H Bond Activation – Photoinduced Delivery of Nitric Oxide and NO-Mediated Antiproliferation Activity Studies

Rajan Kumar,<sup>[a]</sup> Anjlika Yadav,<sup>[b]</sup> Anand Ratnam,<sup>[a]</sup> Sushil Kumar,<sup>[a]</sup> Manju Bala,<sup>[a]</sup> Debpali Sur,<sup>[b]</sup> Shikha Narang,<sup>[a]</sup> Udai P. Singh,<sup>[a]</sup> Prabhat K. Mandal,<sup>\*,[b]</sup> and Kaushik Ghosh<sup>\*,[a]</sup>

**Abstract:** The azo dye methyl red, which has carboxylato and azo functional groups, was used as a ligand for the synthesis of the cyclometalated Ru<sup>III</sup> complex [Ru(L<sup>1</sup>)(PPh<sub>3</sub>)<sub>2</sub>Cl] (**1**, L<sup>1</sup>H<sub>2</sub> = 2-[[4-(dimethylamino)phenyl]diazenyl]benzoic acid) through C–H bond activation. Complex **1** was treated with nitric oxide to afford the organometallic ruthenium nitrosyl complex [Ru(L<sup>2</sup>H)(PPh<sub>3</sub>)<sub>2</sub>(NO)Cl][ClO<sub>4</sub>] (**1a**, L<sup>2</sup>H = 2-[[4-(dimethylamino)-3-nitrophenyl]diazenyl]benzoic acid). The molecular structures of

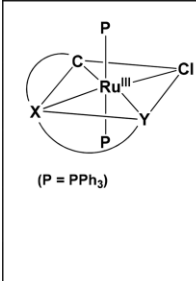
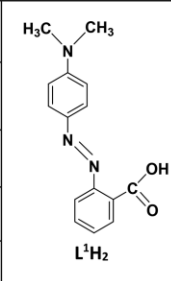
**1**·CH<sub>3</sub>OH and **1a**·CH<sub>3</sub>OH were determined by X-ray crystallography. The diamagnetic complex **1a** with S = 0 ground state was studied by <sup>1</sup>H and <sup>31</sup>P NMR spectroscopy. In the nitrosyl complex, the coordinated NO is photolabile under UV and visible light, and the liberated NO was trapped by reduced myoglobin. The NO, photoreleased under visible light, was utilized in anti-proliferation activity studies on human (A549, HEK293T, and HeLa) and mouse (NIH3T3) cancer cell lines.

## Introduction

In recent years, considerable attention has been paid to the biological chemistry of nitric oxide.<sup>[1,2]</sup> Owing to the extreme importance of this diatomic molecule, the Nobel Prize in Physiology or Medicine was awarded in 1998 for discoveries concerning NO. Nitric oxide has been accepted as an important signaling molecule in several biological processes such as blood-pressure regulation, neurotransmission, immune response, and cellular apoptosis in different cells and tissues.<sup>[1,2]</sup> At the cellular level, NO is produced from L-arginine through catalysis by NO synthase (NOS), and several concentration-dependent activities of NO have been discovered.<sup>[2,3]</sup> In recent years, the target-specific delivery of NO and the scavenging of NO by metal complexes have become important areas in chemical and biochemical research.<sup>[4]</sup> Molecules that can deliver NO upon illumination with light are important for photodynamic therapy (PDT).<sup>[5]</sup>

We have been working with organometallic ruthenium(III) complexes and reported organometallic ruthenium nitrosyl complexes. An evaluation of our previous studies<sup>[6]</sup> (Scheme 1) clearly indicated the necessity of at least one hard donor in the bidentate ligand framework to synthesize cyclometalated ruthenium compounds for the synthesis of organometallic ruth-

enium nitrosyls. The carboxylato (–COO) oxygen atom is a hard donor and stabilizes higher metal oxidation states.<sup>[7]</sup> Hence, we chose methyl red (L<sup>1</sup>H<sub>2</sub>), an azo dye, for our present study (Scheme 1). For the synthesis, we adopted the following synthetic strategy to explore two important aspects: (1) the synthesis of a metal–carbon bond through the presence of a hard donor in the ligand framework to ensure Ru–C bond formation; (2) the investigation of NO reactivity with the same complex as the metal complex should absorb in the visible range because of the presence of the azo function in the ligand framework.

|  | X                  | Y                        | Refs.     |  |
|--|--------------------|--------------------------|-----------|---|
|  | N <sub>azo</sub>   | O <sub>phenol</sub>      | 6a        |   |
|  | N <sub>imine</sub> | O <sub>phenol</sub>      | 6b,c,d    |   |
|  | N <sub>amide</sub> | N <sub>pyridine</sub>    | 6e        |   |
|  | N <sub>azo</sub>   | O <sub>carboxylato</sub> | this work |   |

Scheme 1. Donors (X and Y) in bidentate ligands.

The idea for the present study originated from some recent reports on nitric oxide and its antitumor activity studies. Shami and co-workers reported<sup>[8–10]</sup> that NO has a direct cytotoxic effect on tumor cells. They mentioned that NO leads to the apoptosis of tumor cells through the posttranslational modification of several important proteins. Keefer and co-workers supported the work of Shami and co-workers through the synthesis of similar molecules and reported NO-induced apoptosis through DNA damage.<sup>[11,12]</sup> On the other hand, Xu and co-

[a] Department of Chemistry, Indian Institute of Technology, Roorkee, Roorkee 247667 Uttarakhand, India  
E-mail: ghoshfcy@iitr.ernet.in

[b] Department of Biotechnology, Indian Institute of Technology, Roorkee, Roorkee 247667, Uttarakhand, India  
E-mail: pkm31fht@iitr.ac.in

Supporting information for this article is available on the WWW under <https://doi.org/10.1002/ejic.201700839>.

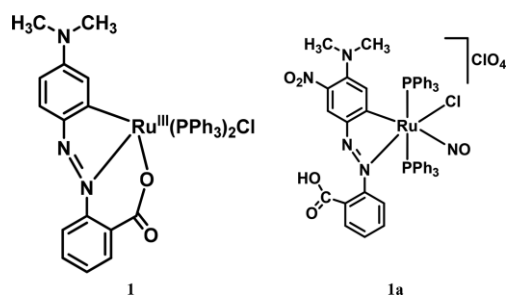
workers mentioned nitric oxide as a “mysterious labile factor” with pleotropic effects and found contradictory effects of NO in terms of antitumor activity.<sup>[13]</sup>

Recently, Mascharak and co-workers reported some ruthenium nitrosyl complexes with strongly colored dye molecules as ligands to enhance the photosensitivity of the Ru–NO moiety in the visible range ( $\lambda_{\text{max}} = 500\text{--}600\text{ nm}$ ).<sup>[14–16]</sup> Da Silva and co-workers also synthesized ruthenium nitrosyl complexes with different ligands that showed sensitivity towards visible light.<sup>[17]</sup> Although several laboratories reported ruthenium nitrosyl complexes that could release NO under visible light, the biological effects of those molecules have not been tested yet. Recently, Liu and co-workers reported the cytotoxic effects of NO released by a ruthenium nitrosyl complex upon visible-light illumination.<sup>[18]</sup> The photosensitivity of a metal nitrosyl depends mainly on the location of the  $d_{\pi}(\text{M}) \rightarrow \pi^*(\text{NO})$  transition in its electronic absorption spectrum.<sup>[14,19]</sup> We also reported organometallic ruthenium nitrosyl complexes with the photolabile nitrosyl ligand.<sup>[6]</sup> The presence of an azo function was important for the photolability of the coordinated NO under visible light. Several research groups (including ours) have explored the different types of photoactive ruthenium nitrosyl complexes.<sup>[2,20,21]</sup> The ruthenium nitrosyl complexes with a {Ru–NO}<sup>6</sup> moiety are more stable and release NO in a predictable manner during illumination. We have reported the nitrosyl complexes  $[\text{Ru}(\text{L}^{\text{SB}2}\text{H})(\text{PPh}_3)_2(\text{NO})\text{Cl}][\text{ClO}_4]$  [ $\text{HL}^{\text{SB}2} = 2\text{-(4-chlorobenzylideneamino)-4-nitrophenol}$ ] and  $[\text{Ru}(\text{L}^{\text{AZ}2}\text{H})(\text{PPh}_3)_2(\text{NO})\text{Cl}][\text{ClO}_4]$  [ $\text{L}^{\text{AZ}2} = 4\text{-methyl-2-nitro-6-(}p\text{-tolylidiazanyl)phenol}$ ], which released the coordinated NO under visible light (tungsten lamp, 60 W), but the rate of photodissociation of the nitrosyl complex containing an azo group was higher than that of the complex without an azo group.<sup>[6a]</sup> The ruthenium complexes  $[\text{Ru}(\text{L}^{\text{SB}3}\text{H})(\text{PPh}_3)_2(\text{NO})\text{Cl}][\text{ClO}_4]$  [ $\text{H}_2\text{L}^{\text{SB}3} = 4\text{-nitro-2-(3-nitrobenzylideneamino)phenol}$ ] and  $[\text{Ru}(\text{L}^{\text{BOX}})(\text{PPh}_3)_2(\text{NO})\text{Cl}][\text{ClO}_4]$  [ $\text{HL}^{\text{BOX}} = 5\text{-methyl-7-nitro-2-(3-nitrophenyl)benzoxazole}$ ] also released NO in the presence of visible light.<sup>[6b]</sup> Some ruthenium nitrosyls such as  $\text{K}_2[\text{Ru}(\text{NO})(\text{Cl})_5]$ <sup>[2,22]</sup> and  $[(\text{PaPy}_3)\text{Ru}(\text{NO})][\text{BF}_4]_2$  [ $\text{PaPy}_3\text{H} = N,N\text{-bis(2-pyridylmethyl)amine-}N\text{-ethyl-2-pyridine-2-carboxamide}$ ] have been used in aqueous media to deliver NO to tissues and proteins.<sup>[19a,23]</sup>

However, most ruthenium nitrosyl complexes delivered the NO only in the presence of UV light, and this is a major drawback for the use of these types of complexes as NO donors in biological experiments. As UV light is intrinsically harmful to cellular targets, we investigated other metal nitrosyls that could release NO under visible light. The sensitivity of metal nitrosyl complexes towards visible light ( $\lambda \geq 450\text{ nm}$ ) is a major requirement for NO donation in PDT. However, reports on photoinduced NO delivery by ruthenium complexes under visible light are scarce. Here, we report a ruthenium nitrosyl complex containing an azo group that releases NO very quickly in the presence of visible light, and the released NO is used in biological experiments.

We describe the synthesis and characterization of the new cyclometalated ruthenium(III) complex  $[\text{Ru}(\text{L}^1)(\text{PPh}_3)_2\text{Cl}]$  (**1**,  $\text{L}^1\text{H}_2 = 2\text{-}\{[4\text{-(dimethylamino)phenyl]diazanyl}\}$ benzoic acid; Scheme 2) and the ruthenium nitrosyl complex  $[\text{Ru}(\text{L}^2\text{H})$

$(\text{PPh}_3)_2(\text{NO})\text{Cl}][\text{ClO}_4]$  (**1a**,  $\text{L}^2\text{H} = 2\text{-}\{[4\text{-(dimethylamino)-3-nitrophenyl]diazanyl}\}$ benzoic acid), which can deliver NO on demand under visible light. The molecular structures of **1**·CH<sub>3</sub>OH and **1a**·CH<sub>3</sub>OH were determined by single crystal X-ray diffraction. For the nitrosyl complex, ligand nitration was also observed in the phenyl ring containing the dimethylamino group [at the *ortho* position to  $-\text{N}(\text{CH}_3)_2$ ]. The photolability of the coordinated NO was examined under visible and UV light, and the liberated NO was transferred to the heme iron center of reduced myoglobin. After the photorelease of the coordinated NO from **1a**, we obtained the new cyclometalated ruthenium(III) complex  $[\text{Ru}(\text{L}^2)(\text{PPh}_3)_2\text{Cl}]$  (**1b**). During the coordination and photorelease of NO, the dissociation and reestablishment of the  $-\text{COO}^-$  group with the metal center was analyzed. The photoreleased nitric oxide was utilized in antiproliferation activity studies on human (A549 and HEK293T) and mouse (NIH3T3) cancer cell lines.

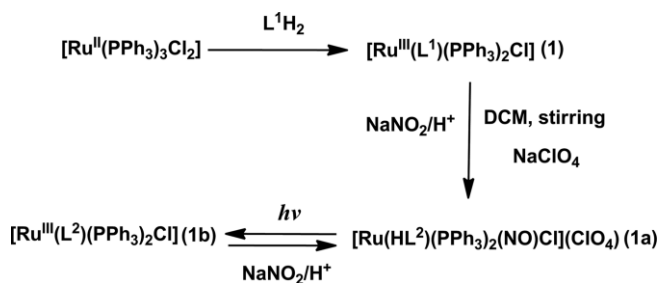


Scheme 2. Ruthenium complexes **1** and **1a**.

## Results and Discussion

### Syntheses

The reaction of  $\text{Ru}(\text{PPh}_3)_3\text{Cl}_2$  with the ligand  $\text{L}^1\text{H}_2$  (1:1) in methanolic solution produced  $[\text{Ru}(\text{L}^1)(\text{PPh}_3)_2\text{Cl}]$  (**1**, Scheme 3). Complex **1** is red-brown and highly soluble in chlorinated solvents such as dichloromethane and chloroform but less soluble in water and methanol. A dichloromethane solution of **1** was treated with an acidified nitrite ( $\text{NaNO}_2$ ) solution with continuous stirring for 2 h, and the resultant orange-yellow nitrosyl compound **1a** was isolated with a perchlorate counteranion (Scheme 3). The nitrosyl complex **1a** is highly soluble in organic solvents such as dichloromethane, acetonitrile, dimethylformamide (DMF), and benzene but less soluble in water. Complexes **1** and **1a** were both recrystallized from dichloromethane/meth-



Scheme 3. Synthetic routes for **1**, **1a**, and **1b**.

anol mixtures. The photoproduct  $[\text{Ru}(\text{L}^2)(\text{PPh}_3)_2\text{Cl}]$  (**1b**, Scheme 3) was obtained when NO was released from the nitrosyl complex **1a**. It was also observed that **1a** could be synthesized from **1b** through the use of acidified nitrite solution (vide infra).

### Description of Structures

The molecular structures of  $[\text{Ru}(\text{L}^1)(\text{PPh}_3)_2\text{Cl}]\cdot\text{CH}_3\text{OH}$  (**1** $\cdot\text{CH}_3\text{OH}$ ) and  $[\text{Ru}(\text{L}^2\text{H})(\text{PPh}_3)_2(\text{NO})\text{Cl}][\text{ClO}_4]\cdot\text{CH}_3\text{OH}$  (**1a** $\cdot\text{CH}_3\text{OH}$ ) are depicted in Figures 1 and 2, respectively. Selected bond lengths and angles are given in Table 1, and the crystallographic data are summarized in Table 2. In the molecular structure of **1** $\cdot\text{CH}_3\text{OH}$ , the carbanion (C2), Cl(1), azo nitrogen (N1), and carboxylato oxygen O(1) atoms constitute the equatorial plane, and the *trans* PPh<sub>3</sub> groups act as axial ligands. The geometry around the Ru<sup>III</sup> center is distorted octahedral, as reflected in the metric parameters (Table 1). In the crystal structure of **1a** $\cdot\text{CH}_3\text{OH}$ , the equatorial plane comprises the carbanion (C2), Cl(1), and azo nitrogen (N1) atoms as well as the NO ligand.

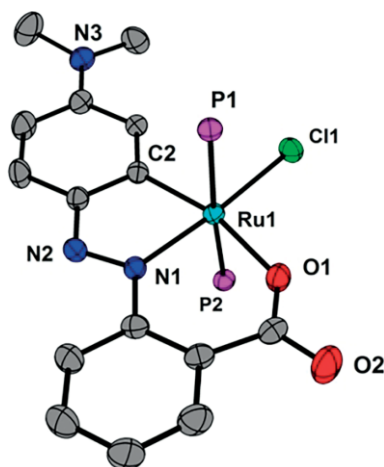


Figure 1. ORTEP diagram (30 % probability level) of **1** $\cdot\text{CH}_3\text{OH}$ . All hydrogen atoms, the phenyl rings of the PPh<sub>3</sub> ligands, and crystallized solvent molecule are omitted for clarity.

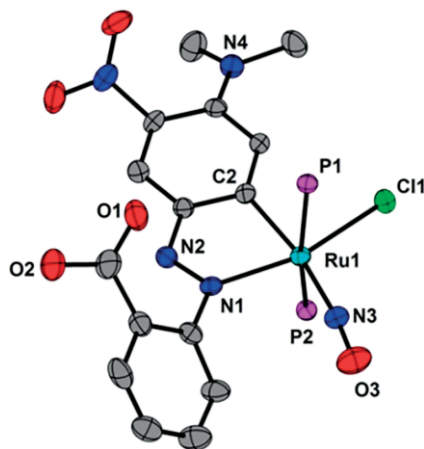


Figure 2. ORTEP diagram (30 % probability level) of the cation of **1a** $\cdot\text{CH}_3\text{OH}$ . All hydrogen atoms, the phenyl rings of the PPh<sub>3</sub> ligands, and crystallized solvent molecule are omitted for clarity.

However, after nitrosylation, the phosphine ligands were intact at axial positions *trans* to each other. Interestingly, in **1a** $\cdot\text{CH}_3\text{OH}$ , the carboxylate oxygen atom (O1) was not bound to the metal center and gave rise to a carboxylic function. In our previous reports,<sup>[6a,6b,6c]</sup> we explored the detachment of phenolato oxygen atoms in the same manner during interactions with NO.

Table 1. Selected bond lengths [Å] and angles [°] of **1** $\cdot\text{CH}_3\text{OH}$  and **1a** $\cdot\text{CH}_3\text{OH}$ .

| Bond lengths [Å]                      |            | Bond angles [°]  |            |
|---------------------------------------|------------|------------------|------------|
| <b>1</b> $\cdot\text{CH}_3\text{OH}$  |            |                  |            |
| Ru(1)–Cl(1)                           | 2.3444(10) | N(1)–Ru(1)–Cl(1) | 175.25(8)  |
| Ru(1)–C(2)                            | 2.009(4)   | N(1)–Ru(1)–C(2)  | 77.94(13)  |
| Ru(1)–N(1)                            | 2.065(3)   | Cl(1)–Ru(1)–P(1) | 87.17(4)   |
| Ru(1)–O(1)                            | 2.075(3)   | C(2)–Ru(1)–P(1)  | 89.67(11)  |
| Ru(1)–P(1)                            | 2.4176(10) | N(1)–Ru(1)–P(2)  | 93.41(9)   |
| Ru(1)–P(2)                            | 2.3944(10) | P(1)–Ru(1)–P(2)  | 174.97(4)  |
|                                       |            | C(2)–Ru(1)–O(1)  | 163.97(13) |
|                                       |            | O(1)–Ru(1)–N(1)  | 86.08(11)  |
| <b>1a</b> $\cdot\text{CH}_3\text{OH}$ |            |                  |            |
| Ru(1)–Cl(1)                           | 2.3655(15) | N(1)–Ru(1)–Cl(1) | 163.68(13) |
| Ru(1)–C(2)                            | 2.088(5)   | N(1)–Ru(1)–C(2)  | 75.77(19)  |
| Ru(1)–N(1)                            | 2.125(4)   | Cl(1)–Ru(1)–P(1) | 83.04(5)   |
| Ru(1)–P(1)                            | 2.4607(16) | C(2)–Ru(1)–P(1)  | 88.37(15)  |
| Ru(1)–P(2)                            | 2.4370(15) | N(1)–Ru(1)–P(2)  | 94.44(12)  |
| Ru(1)–N(3)                            | 1.791(5)   | P(1)–Ru(1)–P(2)  | 166.77(5)  |
| N(3)–O(3)                             | 1.159(6)   | C(2)–Ru(1)–N(3)  | 170.6(2)   |
|                                       |            | Ru(1)–N(3)–O(3)  | 172.3(5)   |

In **1** $\cdot\text{CH}_3\text{OH}$ , the Ru–C(2) [2.009(4) Å] bond length is consistent with the values reported previously<sup>[5a,17]</sup> and very similar to that reported by Bhattacharya and co-workers.<sup>[24]</sup> The Ru–O(1)<sup>[25]</sup> and Ru–P<sup>[26,27]</sup> bond lengths are also close to the values reported previously. In the nitrosyl complex **1a** $\cdot\text{CH}_3\text{OH}$ , the Ru–N<sub>NO</sub> bond length [1.791(5) Å] is also similar to the values reported previously.<sup>[6a,6b]</sup> The NO stretching frequencies ( $\nu_{\text{NO}}$ ,  $\tilde{\nu} \approx 1820 \text{ cm}^{-1}$ , vide infra) and N–O bond length are also consistent with previously reported values.<sup>[14,6b]</sup> The Ru–N and N–O bond lengths as well as the Ru–N–O angle<sup>[6a,28,29]</sup> (ca. 172° for **1a** $\cdot\text{CH}_2\text{Cl}_2$ ) revealed the  $\pi$ -acceptor characteristics<sup>[30]</sup> of the coordinated NO<sup>+</sup> ligand in the complex and demonstrated the {Ru<sup>II</sup>–NO<sup>+</sup>}<sup>6</sup> description of the {RuNO}<sup>6</sup> moiety (*S* = 0 ground state).<sup>[6a,6b,6c]</sup>

The binding of the bidentate ligand to the ruthenium center and the concomitant Ru–C bond formation were authenticated by the X-ray crystal structure of **1**. It is important to note that the bidentate ligand afforded C–H bond activation and a metal–carbon bond was established. Hence, the bidentate ligand became tridentate through the formation of a ruthenium–carbon bond, as we speculated. The reaction with NO resulted in the dissociation of the carboxylato function from the metal center, and the ligand became bidentate again through the coordinated carbanion and azo functions. The nitration of the phenyl ring was also observed at the carbon atom *trans* to the carbanion.<sup>[6b]</sup> During this reaction, there are two active reagents, NO<sub>2</sub> and NO<sub>2</sub><sup>+</sup>. For phenols, it has been reported that the reaction will proceed through a free-radical pathway, but the reaction will go through the electrophilic pathway for simple aromatics.<sup>[6e]</sup> In our system, radical formation is not possi-

Table 2. Crystal data and structural refinement parameters for **1**·CH<sub>3</sub>OH and **1a**·CH<sub>3</sub>OH.

|  | <b>1</b> ·CH <sub>3</sub> OH  | <b>1a</b> ·CH <sub>3</sub> OH  |
|--|---|--|
| Empirical formula  | C <sub>52</sub> H <sub>46</sub> ClN <sub>3</sub> O <sub>4</sub> P <sub>2</sub> Ru | C <sub>52</sub> H <sub>46</sub> Cl <sub>2</sub> N <sub>5</sub> O <sub>10</sub> P <sub>2</sub> Ru |
| Formula weight   | 975.38  | 1134.85  |
| Temperature [K]  | 296(2)  | 296(2)   |
| $\lambda$ [Å] (Mo-K $\alpha$ )                                   | 0.71073   | 0.71073  |
| Crystal system   | monoclinic  | monoclinic   |
| Space group  | <i>P</i> 2 <sub>1</sub> / <i>n</i>  | <i>P</i> 2 <sub>1</sub> / <i>n</i>   |
| <i>a</i> [Å]   | 11.9810(2)  | 14.053(4)  |
| <i>b</i> [Å]   | 18.9911(4)  | 18.025(4)  |
| <i>c</i> [Å]   | 20.2552(4)  | 20.167(4)  |
| $\alpha$ [°]   | 90.00   | 90.00  |
| $\gamma$ [°]   | 90.00   | 90.00  |
| $\beta$ [°]  | 96.7930(10)   | 94.276(6)  |
| <i>V</i> [Å <sup>3</sup> ]                                       | 4576.36(15)   | 5094(2)  |
| <i>Z</i>   | 4   | 4  |
| $\rho_{\text{calcd.}}$ [g cm <sup>-3</sup> ]                     | 1.416   | 1.480  |
| <i>F</i> (000)   | 2008.0  | 2324.0   |
| $\theta$ range   | 1.47–26.43  | 1.52–26.43   |
| Index ranges   | –15 < <i>h</i> < 14, –23 < <i>k</i> < 23, –25 < <i>l</i> < 25                     | –17 < <i>h</i> < 17, –22 < <i>k</i> < 22, –25 < <i>l</i> < 25                                    |
| Data/restraints/parameters                                       | 9404/0/571  | 10491/0/653  |
| GOF <sup>[a]</sup> on <i>F</i> <sup>2</sup>                      | 0.914   | 1.323  |
| <i>R</i> 1 <sup>[b]</sup> [ <i>I</i> > 2 $\sigma$ ( <i>I</i> )]  | 0.0436  | 0.0719   |
| <i>R</i> 1 [all data]  | 0.0862  | 0.1155   |
| <i>wR</i> 2 <sup>[c]</sup> [ <i>I</i> > 2 $\sigma$ ( <i>I</i> )] | 0.1179  | 0.1963   |
| <i>wR</i> 2 [all data]   | 0.1506  | 0.2181   |

[a] GOF =  $\{\sum[w(F_o^2 - F_c^2)^2]/(M - N)\}^{1/2}$  (*M* = number of reflections, *N* = number of parameters refined). [b] *R*1 =  $\sum||F_o| - |F_c||/\sum|F_o|$ . [c] *wR*2 =  $\{\sum[w(F_o^2 - F_c^2)^2]/\sum(F_o^2)\}^{1/2}$ .

ble; therefore, the ring nitration will probably proceed by the electrophilic route at the benzene ring. The photolytic cleavage of NO reestablishes the ruthenium carboxylato bond, and the ligand remains tridentate.

### Spectroscopic Studies

The electronic spectra of the free ligand (methyl red) and complex **1** in dichloromethane are shown in Figures S1 and S2, respectively. Methyl red exhibits a strong band at  $\lambda = 490$  nm, which was assigned to mixed *n*- $\pi^*$  and  $\pi$ - $\pi^*$  transitions.<sup>[31]</sup> For **1**, we observed charge-transfer bands near  $\lambda = 510$  and 590 nm, which are probably due to ligand-to-metal charge-transfer (LMCT) transitions.<sup>[6b,32,33]</sup> The nitrosyl complex **1a** is red-yellow, and its electronic spectrum is displayed in Figure S2. Complex **1a** also exhibited one strong band at  $\lambda \approx 498$  nm, which was attributed to a metal-to-ligand charge-transfer (MLCT) transition of the  $d\pi(\text{Ru}) \rightarrow \pi^*(\text{NO})$  type, and this transition is responsible for the photolability of the {RuNO}<sup>6</sup> moiety.<sup>[19c,20,34,35]</sup> Similar observations were reported by Robertson and co-workers;<sup>[36]</sup> however, these spectral features were assigned on the basis of the previously reported data. For **1b**, two charge-transfer transitions appeared near  $\lambda = 452$  and 523 nm. These bands are probably the result of LMCT transitions.<sup>[6b,32,33]</sup> The band near  $\lambda = 380$  nm is probably due to intraligand *n*- $\pi^*$  and  $\pi$ - $\pi^*$  transitions involving the azo function. Owing to the ligand nitration at the phenyl ring containing the -N(CH<sub>3</sub>)<sub>2</sub> group, the absorption bands of **1b** were blueshifted compared with those of the corresponding precursor complex **1** (Figure S4).

In the IR spectrum of **1a**, the  $\nu_{\text{NO}}$  stretching frequency was found at  $\tilde{\nu} \approx 1820$  cm<sup>-1</sup>; therefore, the complex is of the {Ru<sup>II</sup>-NO<sup>+</sup>}<sup>6</sup> type.<sup>[34,35,37]</sup> The IR peaks at  $\tilde{\nu} = 1095$  and

610 cm<sup>-1</sup> clearly revealed the presence of the perchlorate counteranion in **1a**.<sup>[6a,6b]</sup> Complex **1a** showed a few bands in the range  $\tilde{\nu} = 1290$ –1380 cm<sup>-1</sup>, which were assigned to probable ring nitration.<sup>[6a]</sup> For both **1** and **1a**, the peaks at  $\tilde{\nu} \approx 745$ , 695, and 520 cm<sup>-1</sup> confirmed the presence of axial PPh<sub>3</sub> ligands (Figures S5 and S6).<sup>[6]</sup>

Complex **1a** is diamagnetic, as confirmed by <sup>1</sup>H and <sup>31</sup>P NMR spectroscopy (Figures S7 and S8). In the <sup>1</sup>H NMR spectrum of **1a**, the expected multiple signals were observed in the range  $\delta = 8.5$ –5.5 ppm, and a signal for six protons was observed at  $\delta = 2.5$  ppm owing to the presence of two methyl groups. The singlet at  $\delta \approx 23.0$  ppm in the <sup>31</sup>P NMR spectrum of **1a** clearly indicated the presence of two *trans* PPh<sub>3</sub> groups.<sup>[6,38]</sup> The quantum yields ( $\varphi$ ) for **1a** were determined from the decrease in the absorption band at  $\lambda \approx 498$  nm in the presence of UV light ( $\lambda_{\text{irr}} = 365$  nm) and visible light (100 W) and were found to be  $0.017 \pm 0.001$  and  $0.013 \pm 0.001$ , respectively, in dichloromethane solution. The quantum yield of **1a** is similar to those of some other ruthenium nitrosyl complexes, as shown in Table 3.<sup>[6b,39]</sup>

The electron paramagnetic resonance (EPR) spectrum of the trivalent ruthenium complex **1** with a low-spin d<sup>5</sup> one-electron configuration was recorded in dichloromethane/toluene (1:1) glassy solution (77 K) and is displayed in Figure 3. Complex **1** showed three distinct lines with three different *g* values; therefore, the EPR spectrum indicates the distortion of the C(NO)Cl(P)<sub>2</sub> coordination sphere around the metal center away from octahedral symmetry. The average *g* value was 2.004. The presence of three *g* values ( $g_x \neq g_y \neq g_z$ ;  $g_x = 1.825$ ,  $g_y = 2.002$ ,  $g_z = 2.173$ ) indicates rhombic distortion in **1**.<sup>[33a]</sup> The rhombicity of the spectrum indicates an asymmetric electronic environment around the ruthenium center in the complex.<sup>[27,41]</sup> This

Table 3. Quantum yields ( $\phi$ ) of different {Ru–NO}<sup>6</sup> complexes in different solvents.<sup>[a]</sup>

| Complex   | $\phi$ ( $\lambda_{irr}$ , nm) | Solvent                     |
|---|--------------------------------|-----------------------------|
| This work, <b>1a</b>  | 0.017 ± 0.001 (365)            | DCM                         |
| [Ru(LSB <sup>2</sup> H)(PPh <sub>3</sub> ) <sub>2</sub> (NO)Cl]ClO <sub>4</sub> <sup>[6b]</sup>   | 0.017 ± 0.001 (365)            | CH <sub>3</sub> CN          |
| [Ru(L <sup>BOx</sup> )(PPh <sub>3</sub> ) <sub>2</sub> (NO)Cl]ClO <sub>4</sub> <sup>[6b]</sup>  | 0.012 ± 0.001 (365)            | CH <sub>3</sub> CN          |
| [Ru(L)(NO)Cl <sub>2</sub> ] <sup>[38]</sup> HL = <i>N</i> '-phenyl- <i>N</i> '-(pyridin-2-yl)picolinohydrazide  | 0.002 ± 0.001 (365)            | CH <sub>3</sub> CN          |
| [Ru(L <sup>2</sup> )(PPh <sub>3</sub> ) <sub>2</sub> (NO)Cl][ClO <sub>4</sub> ] <sub>2</sub> <sup>[38]</sup> L = 1-phenyl-1-(pyridin-2-yl)-2-(pyridin-2-ylmethylene)hydrazine | 0.003 ± 0.001 (365)            | CH <sub>3</sub> CN          |
| [Ru(L)(PPh <sub>3</sub> ) <sub>2</sub> (NO)][ClO <sub>4</sub> ] <sup>[39]</sup> H <sub>2</sub> L = iminodiacetic acid   | 0.011 ± 0.001 (365)            | DCM                         |
| [Ru(L <sup>2</sup> )(PPh <sub>3</sub> ) <sub>2</sub> (NO)][ClO <sub>4</sub> ] <sup>[39]</sup> H <sub>2</sub> L = pyridine-2,6-dicarboxylic acid                               | 0.012 ± 0.001 (365)            | DCM                         |
| [Ru(TPA)Cl <sub>2</sub> (NO)ClO <sub>4</sub> ] <sup>[40]</sup>  | 0.060 ± 0.030 (365)            | CH <sub>3</sub> CN          |
| [Ru(TPA)Cl <sub>2</sub> (NO)ClO <sub>4</sub> ] <sup>[40]</sup>  | 0.030 ± 0.020 (365)            | DMF                         |
| [Ru(TPA)(ONO)(NO)][PF <sub>6</sub> ] <sub>2</sub> <sup>[40]</sup>   | 0.01(0) ± 0.002(0) (365)       | DMF                         |
| [Ru(TPA)(ONO)(NO)][PF <sub>6</sub> ] <sub>2</sub> <sup>[40]</sup>   | 0.00 (365)                     | CH <sub>3</sub> CN          |
| [Ru(TPA)(urea)(NO)][PF <sub>6</sub> ] <sub>3</sub> <sup>[40]</sup>  | 0.007 ± 0.001 (365)            | DMF                         |
| [Ru(TPA)(urea)(NO)][PF <sub>6</sub> ] <sub>3</sub> <sup>[40]</sup>  | 0.002 ± 0.001 (365)            | H <sub>2</sub> O and oxy-Mb |
| [Ru(H <sub>2</sub> edta)Cl(NO)] <sup>[40]</sup>   | 0.004 ± 0.003(365)             | H <sub>2</sub> O and oxy-Mb |
| [Ru(Hedta)(NO)] <sup>[40]</sup>   | 0.0002 ± 0.0001 (365)          | H <sub>2</sub> O and oxy-Mb |

[a] TPA = tris(2-pyridylmethyl)amine, H<sub>2</sub>edta = ethylenediaminetetraacetic acid, oxy-Mb = oxymyoglobin.

implies that **1** is significantly distorted from ideal octahedral geometry; therefore, the EPR data are consistent with the data obtained from the crystal structure of **1**.

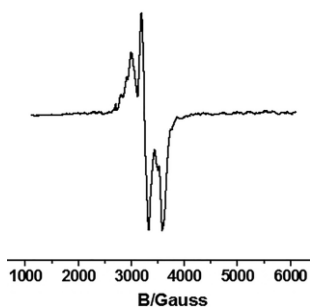


Figure 3. EPR spectrum (X band) of **1** in dichloromethane/toluene (1:1) glass (77 K).

## Electrochemistry

The redox properties of the metal center were measured by cyclic voltammetry (Figure 4) in a dichloromethane solution with 0.1 M *tert*-butylammonium perchlorate (TBAP) as the supporting electrolyte. Complex **1** exhibited two voltammetric responses, one quasireversible oxidation couple (Ru<sup>IV</sup>/Ru<sup>III</sup>) with  $E_{1/2} \approx +0.90$  V and one quasireversible reduction couple (Ru<sup>III</sup>/Ru<sup>II</sup>) with  $E_{1/2} = -0.35$  V versus Ag/AgCl (Figure 4, black line).<sup>[26,33]</sup> These redox processes are quasireversible with large peak-to-peak separations ( $\Delta E_p$ ) of 123 (for **1**) and 101 mV (for **1a**). However, we did not observe any redox couple for **1a**. We observed three cathodic peaks at potentials of ca. -0.32, -0.48, and -0.76 V versus Ag/AgCl (Figure 4, red line). Quasireversible couples (Ru<sup>III</sup>/Ru<sup>II</sup>) were reported at negative potentials for nitrosyl complexes by Mascharak and co-workers.<sup>[19a,20]</sup> Lahiri and co-workers described a ligand-centered (nitric oxide) reduction of {Ru<sup>II</sup>-NO<sup>+</sup>}<sup>6</sup> → {Ru<sup>II</sup>-NO}<sup>7</sup>, which extended to a second one-electron reduction {Ru<sup>II</sup>-NO}<sup>7</sup> → {Ru<sup>II</sup>-NO}<sup>8</sup> and then a third reduction to show three peaks at negative potentials.<sup>[42]</sup> The appearance of an irreversible cathodic peak clearly reveals that NO-centered reduction to afford {RuNO}<sup>7</sup> species, {RuNO}<sup>8</sup> species, and so on is unfavorable.

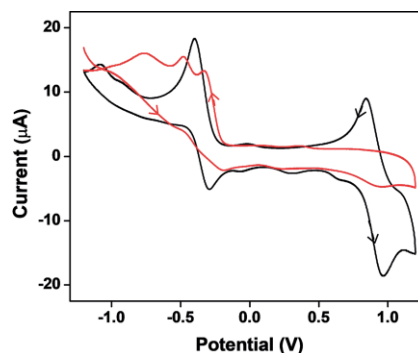


Figure 4. Cyclic voltammograms of 10<sup>-3</sup> M solutions of **1** (black line) and **1a** (red line) in the presence of 0.1 M TBAP with a glassy-carbon working electrode, a Ag/AgCl reference electrode, and a platinum wire auxiliary electrode at a scan rate of 0.1 V s<sup>-1</sup>.

## Photolysis Experiments with the Nitrosyl Complex

The photolysis of the coordinated NO ligand was examined through the exposure of a dichloromethane solution of **1a** to visible (100 W tungsten lamp, Figure 5) and UV light ( $\lambda_{irr} = 365$  nm, Figure S9). A rapid color change from red-yellow to red was observed during the photorelease of NO. No changes were observed in the dark, but we observed a change in the spectrum of **1a** in the presence of visible light. Upon the illumina-

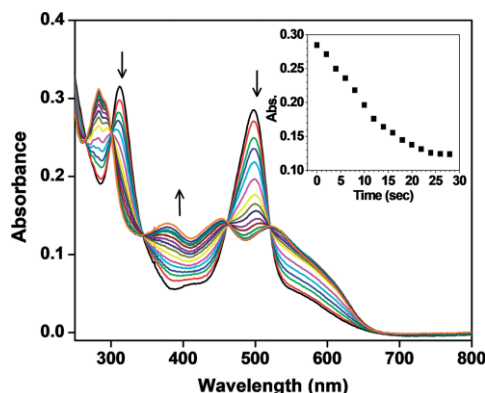
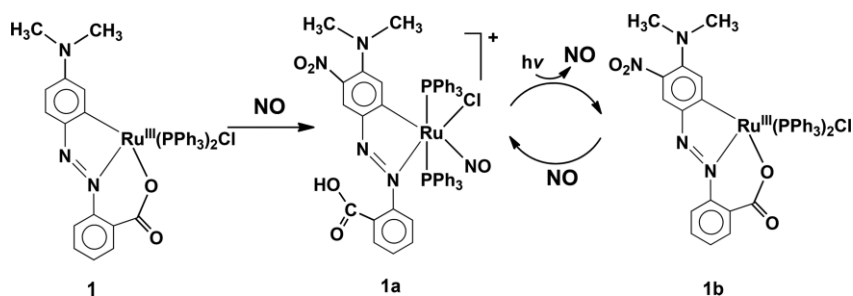


Figure 5. Photocleavage of NO from **1a** (ca. 1.04 × 10<sup>-5</sup> M) in dichloromethane solution under visible light (100 W). Repetitive scans were taken at 2 s intervals. Inset: time-dependent changes in absorbance at  $\lambda = 498$  nm.

Scheme 4. Interconversion of **1a** and **1b**.

tion of a solution of **1a** with visible light, the intensities of the peaks at  $\lambda = 498$  and  $313$  nm decreased, and some new peaks appeared at  $\lambda \approx 523, 452, 380,$  and  $282$  nm. We observed isosbestic points at  $\lambda \approx 518, 460, 343,$  and  $301$  nm (Figure 5). We also discovered that the rate of photodissociation of the coordinated NO was more sensitive to the presence of visible light (100 W tungsten lamp) than to UV light ( $\lambda_{\text{irr}} = 365$  nm). Interestingly, at the end of the photolability experiments with **1a**, we observed the formation of a new complex, **1b**, which was characterized through spectroscopic techniques. Therefore, these results prompted us to investigate the flipping of **1a** and **1b** through NO coordination and photodissociation. Hence, we treated **1b** with acidified nitrite solution and found that **1a** reformed. We then studied the photocleavage of NO from **1a** again. These data indicated that the carboxylate oxygen atom detached from the metal center during the NO interaction, probably owing to the *trans* effect of the carbanion ligand. After the photodissociation of the coordinated NO, the open position at the metal center became available for the carboxylate oxygen atom, and this carboxylate oxygen then attached to the metal center. Therefore, the reestablishment of the Ru–O<sub>carboxylate</sub> bond resulted in the formation of **1b**. Hence, the dissociation and reestablishment of the bond between the metal center and the carboxylate oxygen atom was observed during NO coordination and dissociation (Scheme 4).

### Trapping of NO by Reduced Myoglobin

Nitric oxide trapping experiments were performed through UV/Vis spectroscopy.<sup>[6a,6b,6c]</sup> The photoreleased NO from **1a** was transferred to reduced myoglobin in a phosphate buffer at pH 6.8. The electronic spectrum of oxidized myoglobin (Mb) showed an intense band at  $\lambda = 409$  nm (Soret band). The UV/Vis signal of reduced myoglobin at  $\lambda = 433$  nm was observed after the addition of excess sodium dithionite to the same cuvette. An acetonitrile solution of **1a** was added to the cuvette, and no reaction was observed in the dark; the position of the Soret band was retained. However, when the same mixture was exposed to visible light (100 W) for 30 s, absorption features at  $\lambda = 422$  nm (Figure S10) showed the formation of Mb–NO adduct in solution.<sup>[6a,6b,6c,38]</sup>

### Cytotoxic Effects of **1a** on Human and Mouse Cancer Cell Lines

We investigated the cytotoxic effects of **1a** on the human A549 breast cancer cell line. At a concentration of  $2 \mu\text{M}$ , the complex

showed severe cytotoxicity (Figure 6C) when cells were observed under a microscope after 24 h. The results showed that more than 90 % of the cells detached from the surface and became round (Figure 6C). The treatment of the cells with **1a** in the dark (Figure 6A) and with the control complex **1** (Figure 6B) did not produce any noticeable effects; therefore, the results suggest that **1** is not toxic to the cells, and the cytotoxic effect is caused by NO release upon the visible-light illumination of **1a**. Assays were also performed with human embryonic kidney (HEK293T) and NIH3T3 (mouse) cell lines, and the analysis of the data revealed that the effects were similar to those observed for the A549 cancer cell line (data not shown).

Next, to check the concentration-dependent cytotoxicity of our compound, we treated A549 cells with different concentrations (1, 1.5, 1.75, and  $2 \mu\text{M}$ ) of **1a** (Figure 6D–G). The result showed that a concentration of  $2 \mu\text{M}$  (Figure 6G) is more effective than the other concentrations tested. Next, to check the time-dependent cell death, A549 cells were visualized under a microscope at different time intervals after the treatment of the cells with **1a** (Figure 6H–J). Although the cytotoxic effects started at 3 h, these data showed that it took ca. 24 h for the effective death of most of the cells (Figure 6J).

### Measurement of Dead Cells by Fluorescent Activated Cell Sorting Analysis

Next, we performed fluorescent activated cell sorting (FACS) analysis to measure the exact number of dead cells 24 h after treatment with **1a** (Figure 7C). Again, the effects of **1** in the presence of light (Figure 7A) and **1a** in the dark (Figure 7B) were used as controls. Live–dead gating was adjusted after the cells were stained with propidium iodide (PI). The FACS analysis showed that almost 92 % of the cells were dead 24 h after the treatment with **1a** under visible light to release NO (Figure 7C–E). On the contrary, very negligible cell death was observed for **1** (Figure 7A, D, and E). We observed ca. 20 % dead cells when **1a** was not excited with light (Figure 7B, D, and E). The reason could be that it was not possible to maintain a completely dark environment during handling, and the samples were exposed to a minimum amount of visible light. We speculate that this small amount of light is enough to release NO and that this is sufficient to kill ca. 20 % of the cells. We also performed FACS analysis 8 h after the treatment, and the data showed that ca. 72 % of the cells were dead owing to NO toxicity.

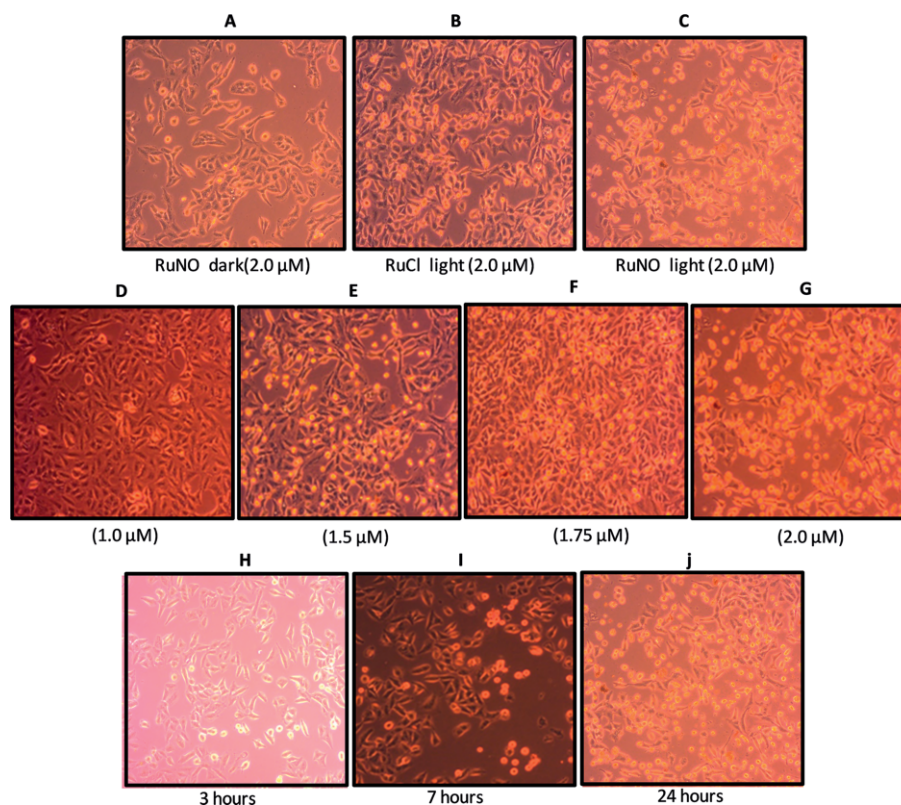


Figure 6. Cytotoxic effects of **1a** on A549 human breast cancer cells. The cells were treated with the indicated concentrations of **1a** and **1** and then exposed to visible light to check the effects of the released NO. Panels A–C: cytotoxic effects of **1a** in the dark, **1** in light, and **1a** in light, respectively, at 2  $\mu\text{M}$  concentration. Panels D–G: cytotoxic effects of **1a** after irradiation with visible light at 1.0, 1.5, 1.75, and 2.0  $\mu\text{M}$  concentration, respectively. Panels H–J: cytotoxic effect of **1a** after 3, 7, and 24 h, respectively.

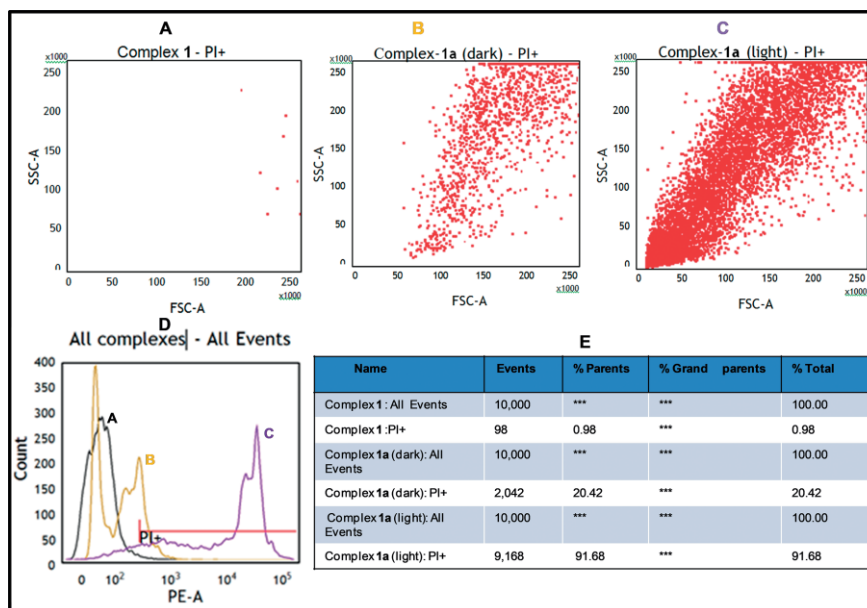


Figure 7. Measurement of the cytotoxic effects of released NO on human cancer cells (HEK293T) through flow cytometry. The prodrug (**1a**) at 0.2  $\mu\text{M}$  final concentration was added to the cells and then illuminated with visible light (100 W) for 5 min. Complex **1** was used as a control to determine the toxicity of the corresponding chloro complex. Complex **1a** without light illumination was used also used as a control. Live–dead gating was performed through PI staining, as only dead cells are stained; 10000 cells (events) were recorded. Panels A–C: dot plots of forward scattering (FSC) vs. side scattering (SSC) of PI-positive cells after treatment with **1** under illumination, **1a** without illumination, and **1a** with illumination, respectively. Panel D: graphical representation of PI-positive cells (y axis) vs. log PI fluorescence intensity (x axis). The black, yellow, and purple peaks represent cells treated with **1** under illumination, **1a** without illumination, and **1a** under illumination, respectively. Panel E: statistical calculation of dead-cell population (PI-positive cells). The percentages of dead cells were 0.98, 20.42, and 91.68 % for **1** under illumination, **1a** without illumination, and **1a** under illumination.

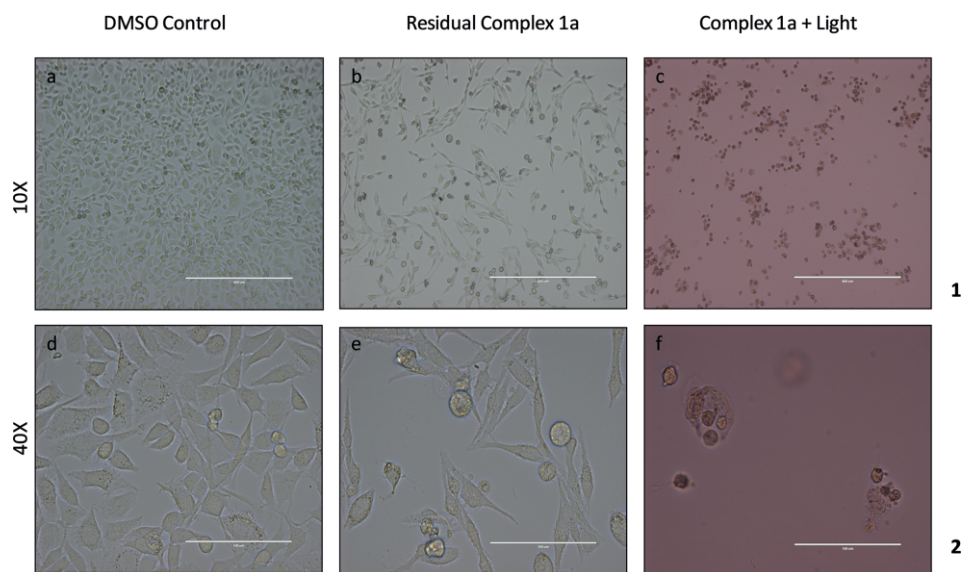


Figure 8. Cytotoxic effects of residual **1a** on HeLa cells. Top: magnified images (10 $\times$ ) of complex-treated cells under an inverted microscope: (a) cells treated with DMSO (control) plus light; (b) cells grown in medium containing **1a**, which was illuminated for 20 min before transfer to the cell medium; (c) cells grown in medium containing illuminated **1a**. The complex-containing culture medium (2  $\mu$ m) was transferred to the cells and then illuminated with white light for 5 min. Bottom: 40 $\times$  magnification images of the same panels.

To verify that our compound itself is not toxic and not responsible for cell death, we illuminated the medium containing **1a** for 20 min and then transferred it to 15 % confluent HeLa cells. The prior illumination of the medium removed all the NO from the complex and left the compound inactive (residual complex). Our results clearly showed that the cells in the control plate [dimethyl sulfoxide (DMSO) medium illuminated with light] were ca. 80 % confluent (Figure 8, Panel 1a), whereas the illuminated residual complex showed nearly 50 % confluence (Figure 8, Panel 1b). Not a single living cell was found in the test disc (Figure 8, Panel 1c; the medium containing the complex was transferred to the cells and illuminated for 5 min to release the NO). This suggests that the cell death is caused by the NO released through the illumination of the complex, and the residual complex has very little cytotoxic effect.

## Conclusions

The major findings and conclusions of the present study are described below. First, the ruthenium(III) cyclometalate [Ru(L<sup>1</sup>)(PPh<sub>3</sub>)<sub>2</sub>Cl] (**1**) derived from the azo dye methyl red was synthesized through C–H activation and characterized by different spectroscopic studies. The molecular structure was determined by X-ray crystallography. Carbanion formation after phenyl C–H activation occurred at the position *trans* to the carboxylato oxygen atom. The results from our previous reports and the present study indicated clearly that a bidentate ligand with one hard donor reacts with Ru(PPh<sub>3</sub>)<sub>3</sub>Cl<sub>2</sub> to afford an organometallic complex after C–H activation. Second, nitric oxide reactivity studies afforded the ruthenium nitrosyl complex [Ru(L<sup>2</sup>H)(PPh<sub>3</sub>)<sub>2</sub>(NO)Cl][ClO<sub>4</sub>] (**1a**), which was characterized by different spectroscopic methods. The molecular structure of the nitrosyl complex was determined by X-ray crystallography. The

nitric oxide coordinated to the metal center *trans* to the carbanion, and the dissociation of the carboxylato function was observed. This may be due to the *trans* effect of the carbanion. Third, ligand nitration at the phenyl group containing the –N(Me)<sub>2</sub> function was authenticated. Fourth, we observed strong charge-transfer (CT) bands in the visible region for **1a**, and the coordinated NO was photolabile under visible and UV light. We investigated the liberation of NO through trapping experiments with reduced myoglobin. During NO coordination, the bond between the ruthenium center and the carboxylato group dissociated, and the same Ru–O bond was reestablished after the liberation of nitric oxide. The presence of an azo function in the ligand framework resulted in NO liberation under visible light; however, we were unable to estimate the amount of nitric oxide released from the molecule with the Griess reagent because of the presence of the azo function in the molecule as well as in the product during the Griess reaction. Fifth, **1a** was utilized for the visible-light-activated delivery of NO and clearly showed antiproliferation activity against human (A549 and HEK293T) and mouse (NIH3T3) cell lines through the controlled release of NO. Sixth, the cytotoxic effect of NO was also investigated with HeLa cells. Our results clearly showed that it is the NO that is cytotoxic and responsible for cell death. Such interesting results are of extreme interest in PDT, and detailed studies on such activity and investigations of the mechanism as well as other biological applications are under progress.

## Experimental Section

**Materials:** All the required chemicals and solvents were reagent grade and used as received. RuCl<sub>3</sub>·3H<sub>2</sub>O and L<sup>1</sup>H<sub>2</sub> (methyl red) were purchased from Loba Chemie Pvt. Ltd., Mumbai, India. The precursor [Ru(PPh<sub>3</sub>)<sub>3</sub>Cl<sub>2</sub>] was prepared by the procedure reported previously.<sup>[43]</sup> Triphenylphosphine (SRL, Mumbai, India), sodium nitrite (Himedia Laboratories Pvt. Ltd., Mumbai, India), anhydrous



disodium hydrogen phosphate (RFCL Ltd. New Delhi, India), and sodium dihydrogen phosphate (Chemport India Pvt. Ltd. Mumbai, India) were used as obtained. Double-distilled water and distilled solvents were used in the experiments. Equine skeletal muscle myoglobin was obtained from Sigma–Aldrich, Steinheim, Germany.

**Physical Measurements:** The IR spectra were obtained from KBr pellets with a Thermo Nicolet Nexus FTIR spectrometer; 16 scans were performed. The electronic absorption spectra of the complexes in dichloromethane and acetonitrile were recorded with a Thermo Scientific (Shimadzu) Evolution 600 UV/Vis spectrophotometer. The  $^1\text{H}$  and  $^{31}\text{P}$  NMR spectra were recorded with a Bruker Avance 500.13 MHz spectrometer with samples in deuterated solvents. Cyclic voltammetric studies were performed with a CH-600C electroanalyzer with samples in dichloromethane with 0.1 M TBAP as the supporting electrolyte. The working electrode, reference electrode, and auxiliary electrode were a glassy carbon electrode, a Ag/AgCl electrode, and Pt wire, respectively. The concentration of the compounds was ca.  $10^{-3}$  M. The ferrocene/ferrocenium couple occurred at  $E_{1/2} = +0.54(70)$  V versus Ag/AgCl (scan rate 0.1 V/s) in dichloromethane under the same experimental conditions.

**X-ray Crystallography:** Red single crystals of **1**·CH<sub>3</sub>OH and **1a**·CH<sub>3</sub>OH were grown by layering hexane over solutions of the complexes in CH<sub>2</sub>Cl<sub>2</sub>/methanol mixtures. The molecular structures showed the presence of one methanol molecule per complex molecule in the lattices. The X-ray data collection and processing were performed with a Bruker Kappa Apex-II CCD diffractometer with graphite-monochromated Mo-K $\alpha$  radiation ( $\lambda = 0.71073$  Å) at 296 K. The crystal structures were solved by direct methods. The structure solutions, refinements, and data output were performed with the SHELXTL program.<sup>[44,45]</sup> All non-hydrogen atoms were refined anisotropically. Hydrogen atoms were placed in geometrically calculated positions and refined in a riding model. The images were created with the DIAMOND program.<sup>[46]</sup>

**[Ru(L<sup>1</sup>)(PPh<sub>3</sub>)<sub>2</sub>Cl] (1):** Ru(PPh<sub>3</sub>)<sub>3</sub>Cl<sub>2</sub> (0.095 g, 0.1 mmol) was added to a methanol solution (35 mL) of L<sup>1</sup>H<sub>2</sub> (0.040 g, 0.15 mmol) and N(C<sub>2</sub>H<sub>5</sub>)<sub>3</sub> (0.020 g, 0.2 mmol), and the mixture was heated under reflux for 4 h at 85 °C with continuous stirring and then cooled to room temperature. The red-brown solid was collected by filtration, washed thoroughly with methanol and diethyl ether, and then dried. Complex **1** was eluted through an alumina column with a dichloromethane/methanol (1:0.1) mixture. Yield: 0.056 g (60 %). C<sub>51</sub>H<sub>43</sub>ClN<sub>3</sub>O<sub>2</sub>P<sub>2</sub>Ru (928.16): calcd. C 65.58, H 4.67, N 4.53; found C 65.72, H 4.61, N 4.46. IR (KBr disk):  $\tilde{\nu} = 1583, 1481, 1430$  ( $\nu_{\text{N=N}}$ ), 1360, 1281, 1220, 1143, 746, 694, 522 ( $\nu_{\text{PPh}_3}$ ) cm<sup>-1</sup>. UV/Vis (CH<sub>2</sub>Cl<sub>2</sub>):  $\lambda_{\text{max}}$  ( $\epsilon$ , M<sup>-1</sup> cm<sup>-1</sup>) = 590 (8601), 511 (15777), 442 (11486), 283 (31817) nm.

**[Ru(L<sup>2</sup>H)(PPh<sub>3</sub>)<sub>2</sub>(NO)Cl][ClO<sub>4</sub>] (1a):** Complex **1** (0.092 g, 0.1 mmol) was dissolved in dichloromethane (30 mL) in a 100 mL round-bottomed flask to afford a brown-red solution. Acidified distilled water (25 mL) was layered over this solution. Sodium nitrite (0.070 g, 1 mmol) was added to the bilayered solution, and the mixture was stirred at room temperature for 2 h to afford a yellow-red solution of **1a**. The dichloromethane layer was separated, and NaClO<sub>4</sub> (excess) and methanol (5 mL) were added to this solution. The mixture was stirred for 1 h and kept in the dark for 3 d to afford **1a** as a crystalline solid. Yield: 0.057 g (52 %). C<sub>51</sub>H<sub>43</sub>Cl<sub>2</sub>N<sub>5</sub>O<sub>9</sub>P<sub>2</sub>Ru (1103.1): calcd. C 55.49, H 3.93, N 6.34; found C 55.63, H 3.92, N 6.26. IR (KBr disk):  $\tilde{\nu} = 1820$  ( $\nu_{\text{NO}}$ ), 1583 ( $\nu_{\text{N=N}}$ ), 1395, 1343, 1098, 610 ( $\nu_{\text{ClO}_4}$ ), 746, 694, 522 ( $\nu_{\text{PPh}_3}$ ) cm<sup>-1</sup>. UV/Vis (CH<sub>3</sub>CN):  $\lambda_{\text{max}}$  ( $\epsilon$ , M<sup>-1</sup> cm<sup>-1</sup>) = 498 (23392), 313 (28144) nm.  $^1\text{H}$  NMR (DMSO, 500 MHz):  $\delta = 8.28$  (s, 1 H), 7.46–7.26 (m, 33 H), 6.44 (d, 1 H), 5.80–5.75 (m, 2 H) ppm.  $^{31}\text{P}$  NMR (DMSO, 500 MHz):  $\delta = 23.28$  ppm.

**Interconversion of 1a and 1b – (i) Conversion of 1a into 1b:** A red-yellow dichloromethane solution of **1a** was exposed to light from a tungsten lamp (100 W). Within 10 min, the solution turned from yellow to red. The solvent was evaporated to afford a red-orange solid, which was washed thoroughly with methanol and diethyl ether.

**(ii) Conversion of 1b into 1a:** Complex **1b** (0.097 g, 0.1 mmol) was dissolved in dichloromethane (25 mL) in a 100 mL round-bottomed flask to give a red solution. Then acidified distilled water (20 mL) was layered over this solution. Sodium nitrite was added to the bilayered solution, and the mixture was stirred at room temperature for 2 h to give a yellow-orange solution of **1a**. The dichloromethane layer was separated, and NaClO<sub>4</sub> (excess) and methanol (5 mL) were added. This solution was stirred for 1 h and kept in the dark for 2–3 d to afford **1a** as a crystalline solid, which was collected by filtration and washed with methanol and diethyl ether.

**Preparation of Phosphate Buffer and Myoglobin Stock Solution:** A 50 mM phosphate buffer solution at pH 6.8 was prepared through the addition of NaH<sub>2</sub>PO<sub>4</sub>·2H<sub>2</sub>O (0.4192 g) and anhydrous Na<sub>2</sub>HPO<sub>4</sub> (0.3283 g) to Milli Q water (50 mL), and the volume was balanced to 100 mL in a volumetric flask. To prepare the myoglobin stock solution, equine skeletal muscle myoglobin (5 mg) was dissolved in the buffer solution (5 mL) described above.

**Quantum-Yield Measurements:** A standard ferrioxalate actinometer (0.006 M solution of potassium ferrioxalate in 0.1 N H<sub>2</sub>SO<sub>4</sub>) was used to determine the intensities of the UV ( $\lambda_{\text{irr}} = 365$  nm) and visible light (100 W tungsten lamp). The quantum yield ( $\Phi_{\text{NO}}$ ) of NO photorelease for **1a** was determined from the decrease in the absorption band at  $\lambda_{\text{max}} \approx 498$  nm upon irradiation with a UV lamp ( $\lambda_{\text{irr}} = 365$  nm) and visible light (100W) and calculated by the procedure reported previously.<sup>[6b]</sup>

**Procedure for Testing the Cytotoxicity of 1a:** Stock solutions of the test and control compounds were prepared freshly in DMSO and filter-sterilized by passage through a 0.22  $\mu\text{m}$  filter. The stability of nitrosyl complex **1a** was examined in Dulbecco's modified Eagle's medium (DMEM, Figure S11), and human (A549 and HEK293T) and mouse (NIH3T3) cell lines were grown in six-well culture plates in DMEM (Hi-Media) supplemented with 10 % fetal bovine serum (FBS) and 5 % CO<sub>2</sub> at 37 °C. To investigate the effects of our complexes, the cells were seeded to achieve ca. 50 % confluence in 24 h. Different concentrations of the test and control compound were then added to the healthy cells. To release NO from the complex, the medium was irradiated with visible light for 5 min. Immediately after light exposure, the cells were transferred to the CO<sub>2</sub> incubator for the indicated times. We utilized inverted microscopy and flow cytometry to examine the cytotoxic effects of the released NO on cancer cells.

The cytotoxic effects of nitric oxide and the complex derived after the photodissociation of nitric oxide were investigated (Figure 8). In this study, we used HeLa cells (human cervical cancer cell line) to examine the cell death caused by the released NO after the illumination of **1a** with light. Around 10<sup>5</sup> HeLa cells were plated in a 35 mm culture disc containing DMEM (2 mL) to obtain ca. 15 % confluency after 6 h. Next, a solution of **1a** (40  $\mu\text{L}$ , stock 1 mM in DMSO) was transferred to a culture disc and mixed, and the medium was illuminated with visible light for 5 min to check the effect of NO on HeLa cell death.

To investigate if the ruthenium complex obtained after illumination (**1b**, supposed to be similar to **1a** but devoid of NO) was nontoxic and, thus, not responsible for cell death at the particular concentration (2  $\mu\text{M}$ ) used, the following experiment was conducted. A

35 mm cell culture disc containing 1 mm complex **1a** in DMEM (2 mL) was illuminated with light for 20 min with the cover kept open inside the cell-culture hood. The medium containing 2  $\mu\text{M}$  **1a** illuminated with light was then transferred to HeLa cells (15 % confluent), which were incubated in a cell-culture incubator for 24 h. An image was captured with the inverted microscope after 24 h, and the dead cells were counted.

## Acknowledgments

K. G. is thankful to Council of Scientific and Industrial Research (CSIR), New Delhi [01(2720)/13/EMR-II dated 17-04-2013] for financial assistance. R. K, A. R., and D. S. are thankful to Ministry of Human Resource Development (MHRD, IIT Roorkee) for their fellowships. S. K, M. B., and S. N. are thankful to Council of Scientific and Industrial Research (CSIR), New Delhi for their fellowships. Anjlika is thankful to Department of Biotechnology (DBT) for her fellowship. P. K. M. is thankful to Department of Science and Technology (DST), New Delhi (EMR/2014/000167, dated 8-10-2015) for financial assistance.

**Keywords:** Ruthenium · Nitrosyl complexes · Structure elucidation · Photochemistry · Antiproliferative activity

- [1] a) *Nitric Oxide: Biology and Pathobiology* (Ed.: L. J. Ignarro), Academic Press, San Diego, CA, **2000**; b) F. P. Rodrigues, Z. A. Carneiro, P. K. Mascharak, C. Curti, R. S. da Silva, *Coord. Chem. Rev.* **2016**, *306*, 701–707; c) L. C. B. Ramos, M. S. P. Marchesi, D. Callejon, M. D. Baruffi, C. N. Lunardi, L. D. Slep, L. M. Bendhack, R. S. Da Silva, *Eur. J. Inorg. Chem.* **2016**, 3592–3597.
- [2] M. J. Rose, P. K. Mascharak, *Curr. Opin. Chem. Biol.* **2008**, *12*, 238–240.
- [3] G. B. Richter-Addo, P. Legzdins, J. Burstyn, *Chem. Rev.* **2002**, *102*, 857–859.
- [4] a) B. R. Cameron, M. C. Darkes, H. Yee, M. Olsen, S. P. Fricker, R. T. Skerlj, G. J. Bridger, N. A. Davies, M. T. Wilson, M. J. Rose, J. Zubieta, *Inorg. Chem.* **2003**, *42*, 1868–1876; b) S. P. Fricker, *Platinum Met. Rev.* **1995**, *39*, 150–159.
- [5] a) P. C. Ford, *Acc. Chem. Res.* **2008**, *41*, 190–200; b) A. K. Patra, R. Afshar, M. M. Olmstead, P. K. Mascharak, *Angew. Chem. Int. Ed.* **2002**, *41*, 2512–2515; *Angew. Chem.* **2002**, *114*, 2622 and references cited therein.
- [6] a) K. Ghosh, S. Kumar, R. Kumar, U. P. Singh, N. Goel, *Organometallics* **2011**, *30*, 2498–2505; b) K. Ghosh, S. Kumar, R. Kumar, U. P. Singh, *Eur. J. Inorg. Chem.* **2012**, 929–938; c) K. Ghosh, S. Kumar, R. Kumar, U. P. Singh, N. Goel, *Inorg. Chem.* **2010**, *49*, 7235–7237; d) K. Ghosh, R. Kumar, S. Kumar, M. Bala, U. P. Singh, *Transition Met. Chem.* **2015**, *40*, 831–837; e) R. Kumar, S. Kumar, M. Bala, A. Ratnam, U. P. Singh, K. Ghosh, *RSC Adv.* **2016**, *6*, 72096–72106 and references therein.
- [7] K. Ghosh, S. Kumar, R. Kumar, U. P. Singh, *J. Organomet. Chem.* **2014**, *750*, 169–175.
- [8] I. Kaur, K. M. Kosak, M. Terrazas, J. N. Herron, S. E. Kern, K. M. Boucher, P. J. Shami, *Pharm. Res.* **2015**, *32*, 1395–1406.
- [9] I. Kaur, M. Terrazas, K. M. Kosak, S. E. Kern, K. M. Boucher, P. J. Shami, *J. Pharm. Pharmacol.* **2013**, *65*, 1329–1336.
- [10] C. Weidensteiner, W. Reichardt, P. J. Shami, J. E. Saavedra, L. K. Keefer, B. Baumer, A. Werres, R. Jasinski, N. Osterberg, A. Weyerbrock, *Nitric Oxide* **2013**, *30*, 17–25.
- [11] L. K. Keefer, *ACS Chem. Biol.* **2011**, *6*, 1147–1155.
- [12] L. K. Keefer, *CCR Connections* **2009**, *3*, 15–17.
- [13] W. Xu, L. Z. Liu, M. Loizidou, M. Ahmed, I. G. Charles, *Cell Res.* **2002**, *12*, 311–320.
- [14] a) M. J. Rose, M. M. Olmstead, P. K. Mascharak, *J. Am. Chem. Soc.* **2007**, *129*, 5342–5343; b) L. Freitag, L. González, *Inorg. Chem.* **2014**, *53*, 6415–6426.
- [15] M. J. Rose, P. K. Mascharak, *Inorg. Chem.* **2009**, *48*, 6904–6907.
- [16] N. L. Fry, B. J. Heilman, P. K. Mascharak, *Inorg. Chem.* **2011**, *50*, 317–324.
- [17] a) M. G. Sauaia, R. G. de Lima, A. C. Tedesco, R. S. da Silva, *Inorg. Chem.* **2005**, *44*, 9946–9951; b) L. P. Franco, S. A. Cicillini, J. C. Biazotto, M. A. Schiavon, A. Mikhailovsky, P. Burks, J. Garcia, P. C. Ford, R. S. da Silva, *J. Phys. Chem. A* **2014**, *118*, 12184–12191.
- [18] H. Xiang, L. An, W. Tang, S. Yang, J. Liu, *Chem. Commun.* **2015**, *51*, 2555–2558.
- [19] a) A. K. Patra, M. M. Olmstead, P. K. Mascharak, *Inorg. Chem.* **2003**, *42*, 7363–7365; b) C. F. Works, C. J. Joher, G. D. Bart, X. Bu, P. C. Ford, *Inorg. Chem.* **2002**, *41*, 3728–3739; c) A. K. Patra, M. J. Rose, K. M. Murphy, M. M. Olmstead, P. K. Mascharak, *Inorg. Chem.* **2004**, *43*, 4487–4495.
- [20] M. J. Rose, A. K. Patra, E. A. Alcid, M. M. Olmstead, P. K. Mascharak, *Inorg. Chem.* **2007**, *46*, 2328–2338.
- [21] M. J. Rose, P. K. Mascharak, *Coord. Chem. Rev.* **2008**, *252*, 2093–2114 and references cited therein.
- [22] a) K. Murphy, J. H. Williams, N. Bettache, T. Bliss, *Neuropharmacology* **1994**, *33*, 1375–1385; b) N. Bettache, T. Carter, J. Corrie, D. Ogden, D. R. Trentham, *Methods Enzymol.* **1996**, *268*, 266–281.
- [23] a) I. Szundi, M. J. Rose, I. Sen, A. A. Eroy-Reveles, P. K. Mascharak, O. Einarsdottir, *Photochem. Photobiol.* **2006**, *82*, 1377–1384; b) M. Madhani, A. K. Patra, T. W. Miller, A. A. Eroy-Reveles, A. J. Hobbs, J. M. Fukuto, P. K. Mascharak, *J. Med. Chem.* **2006**, *49*, 7325–7330.
- [24] F. Basuli, S.-M. Peng, S. Bhattacharya, *Inorg. Chem.* **2001**, *40*, 1126–1133.
- [25] K. Ghosh, S. Kumar, R. Kumar, *Inorg. Chim. Acta* **2013**, *405*, 24–30.
- [26] G. K. Lahiri, S. Bhattacharya, M. Mukherjee, A. K. Mukherjee, A. Chakravorty, *Inorg. Chem.* **1987**, *26*, 3359–3365.
- [27] a) R. Raveendran, S. Pal, *J. Organomet. Chem.* **2007**, *692*, 824–830; b) K. Nagaraju, S. Pal, *J. Organomet. Chem.* **2013**, *737*, 7–11.
- [28] See ref.<sup>[20]</sup>
- [29] R. M. Burns, J. L. Hubbard, *J. Am. Chem. Soc.* **1994**, *116*, 9514–9520.
- [30] a) N. Chanda, S. M. Mobin, V. G. Puranik, A. Datta, M. Niemeyer, G. K. Lahiri, *Inorg. Chem.* **2004**, *43*, 1056–1064; b) S. Sarkar, B. Sarkar, N. Chanda, S. Kar, S. M. Mobin, J. Fiedler, W. Kaim, G. K. Lahiri, *Inorg. Chem.* **2005**, *44*, 6092–6099.
- [31] a) M. S. Masoud, E. A. Khalil, A. M. Hindawy, A. E. Ali, E. F. Mohamed, *Spectrochim. Acta Part A* **2004**, *60*, 2807–2817; b) A. A. Alie El-Deen, A. E.-M. E. El-Askalany, R. Halaoui, B. J. Jean-Claude, I. S. Butler, S. I. Mostafa, *J. Mol. Struct.* **2013**, *1036*, 161–167.
- [32] P. Ghosh, A. Pramanik, N. Bag, G. K. Lahiri, A. Chakravorty, *J. Organomet. Chem.* **1993**, *454*, 237–241.
- [33] a) G. Venkatachalam, R. Ramesh, S. M. Mobin, *J. Organomet. Chem.* **2005**, *690*, 3937–3945; b) S. Kannan, R. Ramesh, Y. Liu, *J. Organomet. Chem.* **2007**, *692*, 3380–3391.
- [34] See ref.<sup>[21]</sup> and references cited therein.
- [35] G. Sauaia, R. G. de Lima, A. C. Tedesco, R. S. Da Silva, *J. Am. Chem. Soc.* **2003**, *125*, 14718–14719.
- [36] Y. Hu, I. Sanchez-Molina, S. A. Haque, N. Robertson, *Eur. J. Inorg. Chem.* **2015**, 5864–5873.
- [37] a) J. B. Godwin, T. J. Meyer, *Inorg. Chem.* **1970**, *10*, 471–474; b) S. S. Borges, C. U. Davanzo, E. E. Castellano, J. Z. Schpector, S. C. Silva, D. W. Franco, *Inorg. Chem.* **1998**, *37*, 2670–2677; c) M. G. Sauaia, F. S. Oliveira, A. C. Tedesco, R. S. da Silva, *Inorg. Chim. Acta* **2003**, *355*, 191–196.
- [38] K. Ghosh, R. Kumar, S. Kumar, J. S. Meena, *Dalton Trans.* **2013**, *42*, 13444–13452.
- [39] K. Ghosh, S. Kumar, R. Kumar, *Eur. J. Inorg. Chem.* **2014**, 1454–1461.
- [40] A. C. Merkle, A. B. McQuarters, N. Lehnert, *Dalton Trans.* **2012**, *41*, 8047–8059.
- [41] R. Raveendran, S. Pal, *J. Organomet. Chem.* **2009**, *694*, 1482–1486.
- [42] S. Maji, B. Sarkar, M. Patra, A. K. Das, S. M. Mobin, W. Kaim, G. K. Lahiri, *Inorg. Chem.* **2008**, *47*, 3218–3227.
- [43] T. A. Stephenson, G. Wilkinson, *J. Inorg. Nucl. Chem.* **1966**, *28*, 945–956.
- [44] G. M. Sheldrick, *Acta Crystallogr., Sect. A: Found. Crystallogr.* **1990**, *46*, 467–473.
- [45] G. M. Sheldrick, *SHELXTL-NT, Version 6.12*, Reference Manual, University of Gottingen, **2000**.
- [46] B. Klaus, *Diamond, Version 1.2c*, University of Bonn, **1999**.

Received: July 12, 2017